

Phase-controlled heat modulation with Aharonov-Bohm interferometers

Sun-Yong Hwang,¹ Björn Sothmann,¹ and Rosa López²

¹*Theoretische Physik, Universität Duisburg-Essen and CENIDE, D-47048 Duisburg, Germany*

²*Institut de Física Interdisciplinària i Sistemes Complexos IFISC (CSIC-UIB), E-07122 Palma de Mallorca, Spain*

(Dated: June 19, 2024)

A heat modulator is proposed based on a voltage-biased Aharonov-Bohm interferometer. Once an electrical bias is applied, Peltier effects give rise to a flow of heat that can be modulated by a magnetic flux. We determine the corresponding temperature changes using a simple thermal model. Our calculations demonstrate that the modulated temperature difference can be as large as 80 mK at base temperature about 600 mK with relative temperature variations reaching 10%. Our model also predicts, quite generally, the emergence of spin-polarized heat flows without any ferromagnetic contacts, if Rashba spin-orbit interaction is combined with the applied magnetic flux, which potentially paves the way towards caloritronic information processing.

I. INTRODUCTION

Manipulating heat currents and temperatures in mesoscopic devices is still an on-going issues in condensed matter physics community [1–3]. Heat dissipations at the nanoscale are usually detrimental phenomena that must be better understood and carefully engineered in order to enhance device functionalities.

Recent efforts to deal with unavoidably present waste heat in nanodevices have led to fruitful progress in novel technologies in the newly developed fields such as spin caloritronics [4] and phase-coherent caloritronics [5, 6], in addition to recently reignited thermoelectrics in the quantum regime [7–9]. In this regards, various caloritronic devices have been proposed that utilize heat in order to construct logical circuits instead of conventional charge degree of freedom. This includes heat interferometers [10–14], diodes [15–18], transistors [19, 20], heat switches [21], circulators [22, 23], thermal memory [24], and mesoscopic refrigerators [25–27]. Central to these phenomena is quantum phase coherence.

Another useful way of thermal managements can be converting electrical work into heat flow via the Peltier effect that can increase or decrease the temperature of reservoirs where the latter case constitutes refrigerators [28–57]. However, controlling heat flow by electrical means always confronts Joule heating effects leading to unidirectional flow of heat with corresponding temperature increases. Thus, an additional switching knob is necessary in order to construct heat and temperature modulators such as magnetic flux [13, 21].

In this paper, we propose a voltage- and phase-controlled heat modulator based on the Aharonov-Bohm interferometer, see Fig. 1. Such an interferometric device has been studied from the perspective of thermoelectric engines and coolers [49, 58–64] while thermal transport has received no attention so far. Furthermore, this type of interferometer has been used to experimentally observe the phase sensitivity [65], Kondo effect [66], partial coherence [67], elastic and inelastic cotunneling [68], and orbital parity symmetry [69]. Therefore, combined with the significant progress in the field of caloritronics [4–6],

our proposal for a coherent heat modulator can be immediately realized with existing experimental technologies.

We calculate electric and heat currents using nonequilibrium Green’s function methods [58, 70] in a model where one arm of the interferometer is connected to the quantum dot molecule with a vibrational degree of freedom. Such a molecular quantum dot can possess intrinsic spin-orbit interaction [71–73] that can be a useful tool for potential spintronic effects. We self-consistently determine the temperature variations at the left reservoir due to electric bias and phase modulation using a phenomenological thermal model [74]. This process includes emergent thermocurrent contributions in every intermediate step accompanying non-stationary thermal gradients until the stationary nonequilibrium states are reached.

The paper is organized as follows. In Sec. II, we detail the device description and theoretical methods. Section

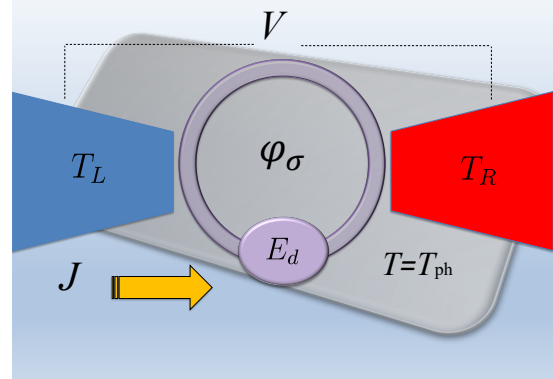


FIG. 1. Device setup based on voltage-biased Aharonov-Bohm interferometer. A spin-dependent phase φ_σ can appear without any magnetic contacts if both the Aharonov-Bohm and Rashba phases are present, see Eq. (5). Heat flow J and the temperature of the left reservoir T_L can be modulated periodically with φ_σ . We assume that the substrate phonon and the right reservoir share the common background temperature $T = T_{\text{ph}} = T_R$ and apply the thermal model, cf. Eqs. (14), (15), (16) to determine the temperature change.

III shows our main results of the thermal modulator with corresponding discussions. We finally give concluding remarks in Sec. IV. Appendix A provides explicit expressions of the self-energy and the lesser Green's function in Eqs. (10) and (11) to make our paper self-contained.

II. MODEL

We consider an Aharonov-Bohm interferometer with a single-level quantum dot embedded in one of the arms. The interferometer is coupled to two electronic reservoirs. In addition, the quantum dot couples to a thermal phononic bath in the substrate, cf. Fig. 1. The Hamiltonian for the proposed setup reads [58, 70]

$$\mathcal{H} = \mathcal{H}_C + \mathcal{H}_D + \mathcal{H}_T, \quad (1)$$

where

$$\mathcal{H}_C = \sum_{\ell=L/R, \mathbf{k}, \sigma} (\varepsilon_{\ell\mathbf{k}\sigma} - \mu_\ell) c_{\ell\mathbf{k}\sigma}^\dagger c_{\ell\mathbf{k}\sigma} \quad (2)$$

depicts the two normal metal electronic reservoirs with local chemical potential μ_ℓ for the left (L) and right (R) side with electron energy $\varepsilon_{\ell\mathbf{k}\sigma}$, momentum \mathbf{k} , spin σ , while

$$\mathcal{H}_D = \sum_{\sigma} E_d d_{\sigma}^\dagger d_{\sigma} + \hbar\omega_0 a^\dagger a + \lambda(a + a^\dagger) \sum_{\sigma} d_{\sigma}^\dagger d_{\sigma} \quad (3)$$

describes an embedded quantum dot with an energy level E_d which is coupled to a phonon bath characterized by an excitation frequency ω_0 and the coupling strength λ between the dot and phonon mode. We envisage the quantum dot as a molecular transistor such as carbon nanotubes or C_{60} [75, 76] with vibrational frequencies of the order of THz. These systems possess intrinsic spin-orbit couplings [77], hence providing the means to generate a quantum mechanical phase in a purely electric manner in addition to the conventional Aharonov-Bohm phase in the presence of magnetic field, see below. In Eq. (3), d_{σ} and a are the corresponding annihilation operators for the dot and the phonon, respectively. Finally, in Eq. (1)

$$\mathcal{H}_T = \sum_{\ell, \mathbf{k}, \sigma} (t_{\ell} c_{\ell\mathbf{k}\sigma}^\dagger d_{\sigma} + \text{H.c.}) + \sum_{\mathbf{k}, \mathbf{p}, \sigma} (W e^{i\varphi_{\sigma}} c_{R\mathbf{p}\sigma}^\dagger c_{L\mathbf{k}\sigma} + \text{H.c.}) \quad (4)$$

accounts for tunneling between the dot and reservoirs, where $c_{\ell\mathbf{k}\sigma}$ is an annihilation operator for electrons with momentum \mathbf{k} and spin σ in the reservoir $\ell = L/R$. Note that in Eqs. (3) and (4), d_{σ} and $c_{\ell\mathbf{k}\sigma}$ are fermionic operators whereas the phonon annihilation operator a in Eq. (3) is a bosonic one. In Eq. (4), t_{ℓ} is the tunneling amplitude between the dot and the reservoirs, i.e., lower arm in Fig. 1, and W describes the direct tunneling process between electronic reservoirs, i.e., upper arm in Fig. 1. The phase factor in Eq. (4) can be written as [71–73]

$$\varphi_{\sigma} = \phi + \text{sgn}(\sigma)\varphi, \quad (5)$$

where $\phi = (e/\hbar)\Phi_B$ is the Aharonov-Bohm phase finite under broken time-reversal symmetry with Φ_B being the magnetic flux. $\varphi = \alpha_R l$ is the Rashba spin-orbit interaction on the dot with α_R and l being respectively the interaction strength and the size of the quantum dot molecule. As we consider a single-level quantum dot, the spin-orbit interaction does not induce spin-flip transitions. Remarkably, Eq. (5) suggests that not only our device functionalities can be controlled by two separate phases either by magnetic (ϕ) or electric (φ) ways, but it can also be used for potential spin caloritronics devices [4] in combination of the two phases even without any ferromagnetic contacts. This spintronic effect originates from an effective Zeeman field induced from the combination of magnetic flux and local Rashba interaction [73].

The spin-resolved charge and heat currents can be respectively calculated from the time evolution of electron number with spin σ , viz. $N_{L\sigma} = \sum_{\mathbf{k}} c_{L\mathbf{k}\sigma}^\dagger c_{L\mathbf{k}\sigma}$, and the energy $\mathcal{H}_{L\sigma} = \sum_{\mathbf{k}} \varepsilon_{L\mathbf{k}\sigma} c_{L\mathbf{k}\sigma}^\dagger c_{L\mathbf{k}\sigma}$ leaving the left reservoir

$$I_{\sigma} = -(ie/\hbar)\langle[\mathcal{H}, N_{L\sigma}]\rangle, \quad (6)$$

$$J_{\sigma} = -(i/\hbar)\langle[\mathcal{H}, \mathcal{H}_{L\sigma}]\rangle - I_{\sigma}(V_L - V_R), \quad (7)$$

where $I_{\sigma}(V_L - V_R)$ corresponds to the Joule heating term. Eqs. (6), and (7) yield via nonequilibrium Green's function methods [58, 78, 79]

$$\begin{pmatrix} I_{\sigma} \\ J_{\sigma} \end{pmatrix} = \frac{1}{\hbar} \int d\varepsilon \begin{pmatrix} e \\ (\varepsilon - \mu) \end{pmatrix} \mathcal{T}_{\sigma}(\varepsilon) [f_L(\varepsilon) - f_R(\varepsilon)], \quad (8)$$

where $\mu = eV + E_F$ and $f_L(\varepsilon) = \{1 + \exp[(\varepsilon - eV - E_F)/k_B T_L]\}^{-1}$ is the Fermi distribution function at the left lead with a local temperature T_L whereas $f_R(\varepsilon) = \{1 + \exp[(\varepsilon - E_F)/k_B T]\}^{-1}$ is that for the right reservoir. We take the Fermi level $E_F = 0$ and the bias voltage configuration $V = V_L$ and $V_R = 0$. We assume the phonon and the right reservoir share the same background temperature $T = T_{\text{ph}} = T_R$. The spin-resolved transmission function in Eq. (8) is explicitly given by [58, 61]

$$\begin{aligned} \mathcal{T}_{\sigma}(\varepsilon) &= \mathcal{T}_{b\sigma} \{ (1 + 2\tilde{\Gamma}_{\sigma} \text{Im} [\mathcal{G}_{\sigma, \sigma}^r]) \\ &+ \tilde{\Gamma}_{\sigma}^2 [1 - \alpha_{\sigma} \cos^2(\varphi_{\sigma})] |\mathcal{G}_{\sigma, \sigma}^r|^2 \} + \tilde{\Gamma}_{\sigma}^2 \alpha_{\sigma} |\mathcal{G}_{\sigma, \sigma}^r|^2 \\ &+ 2\tilde{\Gamma}_{\sigma} \sqrt{\alpha_{\sigma} \mathcal{T}_{b\sigma} (1 - \mathcal{T}_{b\sigma})} \cos(\varphi_{\sigma}) \text{Re} [\mathcal{G}_{\sigma, \sigma}^r], \quad (9) \end{aligned}$$

where $\mathcal{T}_{b\sigma}(\varepsilon) = 4\xi_{\sigma}(\varepsilon)/[1 + \xi_{\sigma}(\varepsilon)]^2$, $\xi_{\sigma}(\varepsilon) = \pi^2 \rho_{L\sigma}(\varepsilon) \rho_{R\sigma}(\varepsilon) W^2$, $\alpha_{\sigma}(\varepsilon) = 4\Gamma_{L\sigma} \Gamma_{R\sigma} / (\Gamma_{L\sigma} + \Gamma_{R\sigma})^2$, $\tilde{\Gamma}_{\sigma}(\varepsilon) = (\Gamma_{L\sigma} + \Gamma_{R\sigma}) / (1 + \xi_{\sigma}(\varepsilon))$, $\Gamma_{\ell\sigma}(\varepsilon) = \pi \rho_{\ell\sigma}(\varepsilon) t_{\ell}^2$ with $\rho_{\ell\sigma}(\varepsilon) = \sum_{\mathbf{k}} \delta(\varepsilon - \varepsilon_{\ell\mathbf{k}\sigma})$. For definiteness, we neglect the spin-polarization of the contacts such that $\Gamma_{\ell\sigma} = \Gamma_{\ell}$ and take the semi-elliptic band for the density of states, i.e., $\rho_{\ell\sigma}(\varepsilon) = \rho_{\ell}(\varepsilon) \propto \sqrt{1 - (\varepsilon/D)^2}$, with which one writes $\xi_{\sigma}(\varepsilon) = \xi(\varepsilon) = \xi_0 [1 - (\varepsilon/D)^2]$. Thus, an energy-independent dimensionless quantity ξ_0 represents a direct tunneling rate only through the upper arm in Fig. 1. For numerical calculations, we fix the half-bandwidth $D = 10k_B T$. We remark that the choice of a

different band, e.g., Lorentzian $1/[1 + (\varepsilon/D)^2]$, does not qualitatively modify the results in our work. In Eq.(9), the retarded Green's function can be written by [60]

$$\mathcal{G}_{\sigma,\sigma}^r(\varepsilon) = [\varepsilon - E_d - \Sigma_{0\sigma}^r(\varepsilon) - \delta\varepsilon_P - \Sigma_{P\sigma}^r(\varepsilon)]^{-1}, \quad (10)$$

exact up to the second order in electron-phonon coupling λ , where $\Sigma_{0\sigma}^r(\varepsilon) = -i\tilde{\Gamma}_\sigma - \tilde{\Gamma}_\sigma\sqrt{\alpha_\sigma\xi_\sigma}\cos(\varphi_\sigma)$ is the self-energy due to couplings to the leads. $\delta\varepsilon_P$ and $\Sigma_{P\sigma}^r(\varepsilon)$ are the energy shift and the self-energy correction arising from the electron-phonon coupling, respectively. The explicit expression for $\delta\varepsilon_P$ reads

$$\delta\varepsilon_P = -\frac{2\lambda^2}{\hbar\omega_0} \sum_{\sigma} \frac{1}{2\pi i} \int d\varepsilon \mathcal{G}_{\sigma,\sigma}^<(\varepsilon), \quad (11)$$

whereas those of $\Sigma_{P\sigma}^r(\varepsilon)$ in Eq. (10) and the lesser Green's function $\mathcal{G}_{\sigma,\sigma}^<(\varepsilon)$ in Eq. (11) are provided in Appendix A. As one can easily notice, the effects of $\delta\varepsilon_P$ and $\Sigma_{P\sigma}^r(\varepsilon)$ are the renormalization of the dot level $E_d \rightarrow E_d + \delta\varepsilon_P$ and the tunnel couplings $\Sigma_{0\sigma}^r(\varepsilon) \rightarrow \Sigma_{0\sigma}^r(\varepsilon) + \Sigma_{P\sigma}^r(\varepsilon)$, respectively. We focus on a noninteracting quantum dot, as our primary interest lies in the interference effects that are revealed through phase dependence. Furthermore, at the mean-field level, interaction only yields a shift in the energy level, hence effectively playing the same role as $\delta\varepsilon_P$ quantitatively. Once the charge and spin currents are determined via Eq. (6) as $I_c = I_\uparrow + I_\downarrow$ and $I_s = I_\uparrow - I_\downarrow$, one can then evaluate the total heat flux J and the spin-polarized heat J_s via Eq. (7), i.e.,

$$J = J_\uparrow + J_\downarrow, \quad (12)$$

$$J_s = J_\uparrow - J_\downarrow, \quad (13)$$

that are of our main interest and can be controlled by phases ϕ or φ , cf. Eq. (5).

In Eq. (8), we have only considered the elastic contribution to the currents although there exists an inelastic term of the order λ^2 containing the phase-dependent term proportional to $\sin\varphi_\sigma$ [79]. We justify this by taking the small value of $\lambda = 0.1k_B T$ in the numerical calculations. Further justification can be made by assuming that this inelastic term can be safely absorbed into the phenomenological equation based on the thermal model, where the heat flow from the substrate can be written by [74]

$$P_{\text{el-ph}} = \Sigma\mathcal{V}(T_L^5 - T_{\text{ph}}^5), \quad (14)$$

where Σ and \mathcal{V} respectively denote the strength of electron-phonon coupling and the volume of the device. We take $\Sigma \simeq 10^9 \text{ WK}^{-5}\text{m}^{-3}$ and $\mathcal{V} \simeq 10^{-20}\text{m}^3$, that are realistic values for a typical mesoscopic setup [1]. Initially, we consider an isothermal situation $T_L = T = T_R$, and since the applied voltage generates the heat flow due to Peltier effect, the temperature of the left lead also changes

$$T_L = T + \delta T, \quad (15)$$

where the amount of change δT can be determined via Eqs. (12) and (14) from the heat balance equation

$$J + P_{\text{el-ph}} = 0. \quad (16)$$

We self-consistently include the emerging thermocurrents whenever the temperature gradient is generated until the stationary solutions of the heat flow J and δT are reached [57]. We will not consider applied thermal gradient across the system, thus the control of heat and temperature in our device are managed with electrical voltages. We also mention that if the dissipative Joule heating contribution becomes large one should in general consider the temperature change of both reservoirs while we have only considered that of left metal for definiteness, following Ref. [57]. Furthermore, the case with strong Coulomb interactions at the quantum dot with an arbitrary strength of the electron-phonon coupling is beyond the scope of this work and hence left as future investigations.

III. RESULTS AND DISCUSSION

Figure 2(a) displays the contour map of the steady heat flow J as functions of an Aharonov-Bohm (AB) phase (ϕ) and an applied voltage (V), in units of $(k_B T)^2/h$. The dotted lines indicate vanishing heat current ($J = 0$) and the dashed lines denote the region where net cooling of the left reservoir can be achieved, i.e., $J > 0$. Notably, the sign of J can be easily controlled by varying the magnetic flux ($\Phi_B \propto \phi$) threaded through the device at a fixed voltage bias. As indicated in Eq. (5), the role of ϕ can be replaced with the Rashba phase φ since an elastic contribution of transmission function only contains terms proportional to $\cos\varphi_\sigma$ hence the role of two phases can be interchanged in the absence of one another. Practically, however, controlling with the magnetic flux will be easier to vary the effects of a phase than by tuning the spin-orbit interaction.

In Fig. 2(b), J is plotted as a function of voltage for several given AB phases. J can be nonzero as the voltage is applied and can become positive, i.e., net cooling effect, until the Joule heating dominates making J with large negative values. Nevertheless, one can notice that at a given voltage, the sign of J can be easily switched with varying ϕ . This is more clearly visible in Fig. 2(c) where we plot it as a function of ϕ for several chosen values of voltage. The direction of heat flow can be conveniently modulated with AB phase as a control knob. It should be noted that there are optimum ranges of V within which periodic sign change of heat is more pronounced since large voltages finally hinder cooling-heating modulation effects invisible due to Joule heating, e.g., $|eV| = k_B T$ in Fig. 2(c). Nevertheless, even in full heating regime characterized by $J < 0$, the amplitude of heat modulation is visibly large which thus induces a large temperature modulation in our device.

We explore now the dependence of temperature modulation δT cf. Eq. (15), on several model parameters such

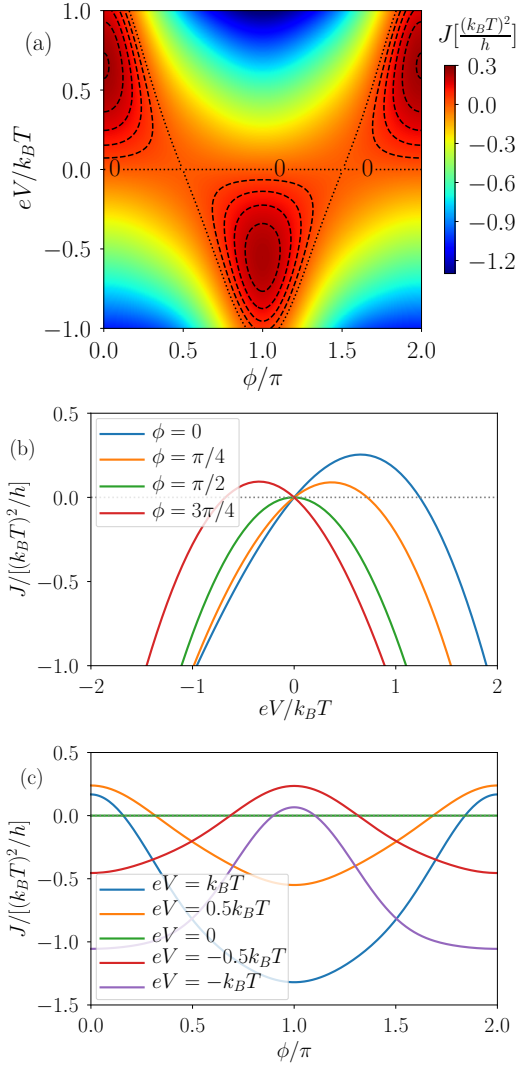


FIG. 2. (a) J versus ϕ and eV . Dotted lines represent a vanishing heat current $J = 0$, while the dashed lines indicate the region where the left reservoir is cooled down, i.e., $J > 0$. (b) and (c) depict cross-sectional views of (a) along the vertical ($\phi = 0, \pi/4, \pi/2, 3\pi/4$) and horizontal axes ($eV/k_B T = 1, 0.5, 0, -0.5, -1$), respectively. Rest of parameters: $E_d = 0.3k_B T$, $\hbar\omega_0 = 0.2k_B T$, $\lambda = 0.1k_B T$, $\Gamma_L = \Gamma_R = 0.5k_B T$, and $\xi_0 = 0.4$, $\varphi = 0 \pmod{2\pi}$.

as the tunnel broadening Γ and the phonon frequency ω_0 as the voltage and the phase are varied. Figure 3 shows such dependences of δT . In particular, Fig. 3(a) shows the accompanying temperature modulation δT , plotted as a function of voltage bias at fixed phases $\phi = \varphi = 0 \pmod{2\pi}$ for selected values of coupling strengths Γ . Unsurprisingly, within a certain range of voltages there exist cooling effects $\delta T < 0$ after which Joule heating largely dominates and hence the temperature increases producing a positive $\delta T > 0$. However, at a fixed V as shown in Fig. 3(b) with $eV = 0.8k_B T$, δT can be periodically modulated with a phase either by ϕ or φ although only the latter example is displayed here. Remarkably, tem-

perature difference between the maximum at $\varphi = \pi$ and the minimum $\varphi = 2n\pi$ (n : integer) can be as large as 80 mK, which is much larger than the experimentally achievable temperature measurement resolution of the order of 0.1 mK [1]. Furthermore, modulations are robust against unintended variations of E_d as can be seen from Fig. 3(b), or put it another way, do not resort to a fine tuning of E_d establishing the shown phenomena mainly from phase effects. The inset of Fig. 3(b) displays effects of a large variations of E_d at $\varphi = 0$ while other parameters fixed. It is shown that for a refrigeration effect to occur at $\varphi = 2n\pi$, there exists a broad range of E_d where $\delta T < 0$. For larger values of $|E_d|$, the temperature finally rises. Figure 3(c) shows the effects of varying background transmission ξ_0 for different values of the phonon frequency at a fixed phase. It is not surprising that δT is rather insensitive to the variation of ω_0 since in our model of weak electron-phonon coupling, the main effect of phonons is a renormalization of the level position and the coupling strengths, cf. Eq. (10). For $\xi_0 \rightarrow 0$, i.e., in the limit where the upper arm is absent in Fig. 1, the sign of δT can change from negative to positive indicating the role of interference for refrigeration effects in this parameter regime. In the inset of Fig. 3(c), the coefficient of thermodynamic uncertainty relation violation [80, 81] \mathcal{C}_T is plotted at $\hbar\omega_0 = 0.2k_B T$ as ξ_0 is varied, where

$$\mathcal{C}_T = 2 \frac{J^2}{S_J} \cdot \frac{k_B}{\sigma_E}, \quad (17)$$

with the heat current noise given by

$$S_J = \frac{1}{h} \int d\varepsilon (\varepsilon - eV)^2 \left\{ \sum_{\sigma} \mathcal{T}_{\sigma}(\varepsilon) \sum_{\ell=L,R} [f_{\ell}(\varepsilon)(1 - f_{\ell}(\varepsilon))] + \sum_{\sigma} \mathcal{T}_{\sigma}(\varepsilon) [1 - \sum_{\sigma} \mathcal{T}_{\sigma}(\varepsilon)] [f_L(\varepsilon) - f_R(\varepsilon)]^2 \right\}, \quad (18)$$

and the entropy production being $\sigma_E = IV/T + J\delta T/T^2$. As shown, the thermodynamic uncertainty relation is not violated, i.e., $\mathcal{C}_T \leq 1$, in our system. However, \mathcal{C}_T becomes maximal, i.e., closer to the violation, roughly when the cooling effects become the largest with $\delta T < 0$, indicating that fluctuations generate less entropy in the refrigeration regime.

In order to quantify the figure of merit for the temperature modulation in our device, we introduce a relative temperature variation defined by [13, 21]

$$\mathcal{R} = \frac{T_L^{\max} - T_L^{\min}}{T_L^{\min}}, \quad (19)$$

where T_L^{\max} (T_L^{\min}) is the maximum (minimum) temperature obtained by the phase modulation, e.g., at $\varphi = \pi$ ($\varphi = 2n\pi$) in Fig. 3(b). \mathcal{R} is plotted in Fig. 3(d) as V is applied for different base temperatures ranged approximately from 500 mK to 1 K, where one could get $\mathcal{R} \sim 10\%$ for optimum conditions. This value is comparable in magnitude to experimentally obtained values

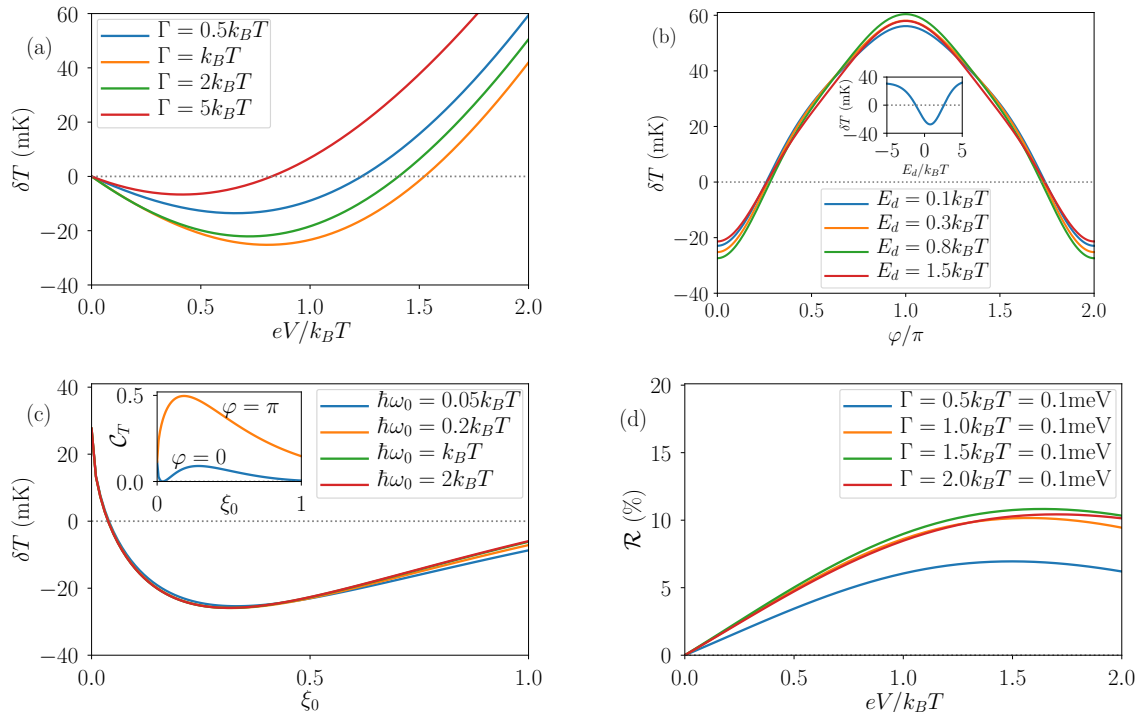


FIG. 3. δT versus (a) eV for various $\Gamma = \Gamma_L = \Gamma_R$ at $\phi = \varphi = 0$, $E_d = 0.3k_B T$, $\hbar\omega_0 = 0.2k_B T$, (b) φ for several E_d at $\phi = 0$, $eV = 0.8k_B T$ and $\Gamma = k_B T$, (c) ξ_0 for several ω_0 at $\phi = \varphi = 0$, $E_d = 0.3k_B T$, $eV = 0.8k_B T$ and $\Gamma = k_B T$ with $T \approx 580$ mK, (d) \mathcal{R} vs. V for various T at a fixed $\Gamma = 0.1$ meV. In (a),(b),(d), we take $\xi_0 = 0.4$ and in all cases, we set $\lambda = 0.1k_B T$. Inset in (b) is a plot as a function of E_d at $\varphi = 0$. Inset in (c) shows \mathcal{C}_T vs ξ_0 at $\hbar\omega_0 = 0.2k_B T$ for $\varphi = 0$ and $\varphi = \pi$ while other parameters are fixed.

[13] as well as a theoretical estimation of high-efficiency thermal switch based on the topological Josephson junction [21], with an added advantage in our setup that we do not need a SQUID geometry with superconducting Josephson junctions.

Finally, we discuss about the spin-polarized heat flow, cf. Eq. (13), which may be relevant to recent developments in spin caloritronics [4] and phase-coherent caloritronics [5, 6] that envisage novel quantum information processing devices based on the generated heat flow. In Fig. 4(a), J_s is shown as functions of two phases that can be respectively controlled magnetically and electrically. As discussed above, one can notice that J_s is symmetric when the role of the magnetic AB phase and the electric Rashba phase are interchanged, cf. Eq. (5), since the cosine function is even and the transmission in Eq. (9) contains terms including only $\cos \varphi_\sigma$. Importantly, for J_s to be nonzero, both phases should be present thus an essential requirement for spintronic effects in the device is a finite magnetic field. Otherwise, everything else involves purely electrical means without any ferromagnetic contacts. Remarkably, both for $J_s > 0$ and $J_s < 0$ regimes, corresponding powers are almost equal in strength in stark contrast to the total heat flux J as shown in Fig. 2(a). This can be more visible in Fig. 4(b) where J_s is plotted as a function of Rashba phase for a fixed $\phi = \pi/2$. As shown, the amplitude and the sign

of J_s signals can be controlled electrically by applying voltage bias across the system for fixed phases.

IV. CONCLUSIONS

We have proposed a heat and temperature modulator based on the mesoscopic Aharonov-Bohm interferometer which is voltage biased. The direction and the amplitude of the heat flow can be easily controlled by either Aharonov-Bohm or Rashba phase with the aid of electrical bias. Correspondingly, temperature variations can be also modulated by the phases working as control knobs. The temperature variations is of the order of 80 mK with accompanying heat flow of the order of hundreds fW. The relative temperature variations can reach 10% which is comparable to reported values in experiments and other theoretical proposals. Our proposal provides an easy manipulation of the heat flow and the temperature variations, both the direction and the amplitude, exploiting the Aharonov-Bohm and Rashba phases. Furthermore, in general cases with both phases present, our device can generate spin-polarized heat flows even without any ferromagnetic leads, that can switch the sign easily by the magnetic flux and the voltage bias. Potentially, this spintronic heat flow can be used for information processing devices in the caloritronic setup. Thus, our results are

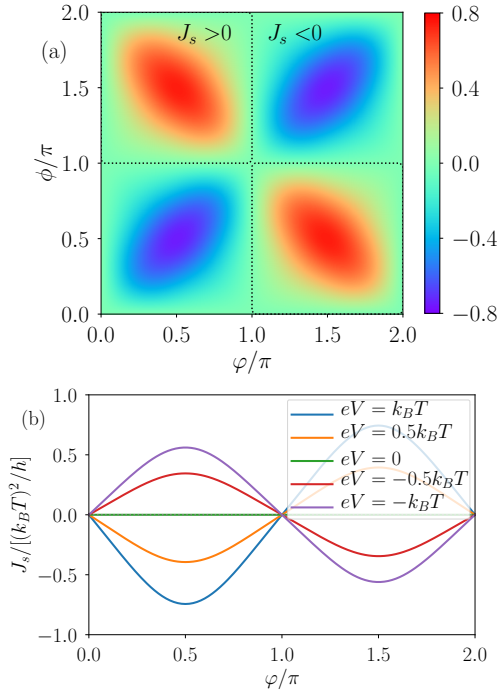


FIG. 4. J_s versus (a) φ and ϕ at $eV = k_B T$, (b) φ for several eV at $\phi = \pi/2$. Parameters are $E_d = 0.3k_B T$, $\hbar\omega_0 = 0.2k_B T$, $\lambda = 0.1k_B T$, $\Gamma_L = \Gamma_R = 0.5k_B T$, and $\xi_0 = 0.4$. Dotted lines indicate the boundary where $J_s = 0$.

strongly relevant to recently proposed novel technologies such as spin and phase-coherent caloritronics.

ACKNOWLEDGMENTS

SYH is so much grateful to J. Niedźwiedzka and W. Wnuczyńska for insightful discussions. We acknowledge financial support from the Ministry of Innovation NRW via the “Programm zur Förderung der Rückkehr des hochqualifizierten Forschungsnachwuchses aus dem Ausland”. R.L. acknowledges the financial support by Grant No. PDR2020/12 sponsored by the Comunitat Autònoma de les Illes Balears through the Direcció General de Política Universitaria i Recerca with funds from the Tourist Stay Tax Law ITS

2017-006, Grants No. PID2020-117347GB-I00, and No. LINKB20072 from the CSIC i-link program 2021. This work has been partially supported by the María de Maeztu project CEX2021-001164-M funded by the MCIN/AEI/10.13039/501100011033.

Appendix A: Lesser Green’s function and the retarded phonon self-energy

The lesser (greater) Green’s function in Eq. (11) is given by

$$\mathcal{G}_{\sigma,\sigma}^{</>}(\varepsilon) = \mathcal{G}_{\sigma,\sigma}^r(\varepsilon)\Sigma_{0\sigma}^{</>}(\varepsilon)\mathcal{G}_{\sigma,\sigma}^{r,*}(\varepsilon), \quad (\text{A1})$$

where $\mathcal{G}_{\sigma,\sigma}^r(\varepsilon) = [\varepsilon - E_d + i\tilde{\Gamma}_\sigma + \tilde{\Gamma}_\sigma\sqrt{\alpha_\sigma\xi_\sigma}\cos(\varphi_\sigma)]^{-1}$,

$$\begin{aligned} \Sigma_{0\sigma}^{<}(\varepsilon) &= \frac{2i}{(1+\xi_\sigma)^2}[(\Gamma_{L\sigma} + \xi_\sigma\Gamma_{R\sigma})f_{L\sigma}(\varepsilon) \\ &\quad + (\Gamma_{R\sigma} + \xi_\sigma\Gamma_{L\sigma})f_{R\sigma}(\varepsilon)] \\ &\quad + \frac{i\Gamma_\sigma}{1+\xi_\sigma}\sqrt{\alpha_\sigma\mathcal{T}_{b\sigma}}\sin(\varphi_\sigma)(f_{L\sigma}(\varepsilon) - f_{R\sigma}(\varepsilon)), \quad (\text{A2}) \end{aligned}$$

and

$$\begin{aligned} \Sigma_{0\sigma}^{>}(\varepsilon) &= -\frac{2i}{(1+\xi_\sigma)^2}[(\Gamma_{L\sigma} + \xi_\sigma\Gamma_{R\sigma})(1 - f_{L\sigma}(\varepsilon)) \\ &\quad + (\Gamma_{R\sigma} + \xi_\sigma\Gamma_{L\sigma})(1 - f_{R\sigma}(\varepsilon))] \\ &\quad + \frac{i\Gamma_\sigma}{1+\xi_\sigma}\sqrt{\alpha_\sigma\mathcal{T}_{b\sigma}}\sin(\varphi_\sigma)(f_{L\sigma}(\varepsilon) - f_{R\sigma}(\varepsilon)). \quad (\text{A3}) \end{aligned}$$

Equipped with lesser and greater Green’s functions, the self-energy correction due to phonon in Eq. (10) can be written as

$$\begin{aligned} \Sigma_{P\sigma}^r(\varepsilon) &= i\lambda^2 \int \frac{d\varepsilon'}{2\pi} \left\{ \left(\frac{\langle aa^\dagger \rangle}{\varepsilon - \hbar\omega_0 - \varepsilon' + i0^+} \right. \right. \\ &\quad \left. \left. + \frac{\langle a^\dagger a \rangle}{\varepsilon + \hbar\omega_0 - \varepsilon' + i0^+} \right) \mathcal{G}_{\sigma,\sigma}^{>}(\varepsilon') \right. \\ &\quad \left. - \left(\frac{\langle aa^\dagger \rangle}{\varepsilon + \hbar\omega_0 - \varepsilon' + i0^+} + \frac{\langle a^\dagger a \rangle}{\varepsilon - \hbar\omega_0 - \varepsilon' + i0^+} \right) \mathcal{G}_{\sigma,\sigma}^{<}(\varepsilon') \right\}, \quad (\text{A4}) \end{aligned}$$

where $\langle a^\dagger a \rangle = \langle aa^\dagger \rangle - 1 = N_{ph} = (e^{\hbar\omega_0/k_B T_{ph}} - 1)^{-1}$ is the Bose-Einstein occupation for the phonon mode.

- [1] F. Giazotto, T. T. Heikkilä, A. Luukanen, A. M. Savin, and J. P. Pekola, Opportunities for mesoscopics in thermometry and refrigeration: Physics and applications, *Rev. Mod. Phys.* **78**, 217 (2006).
- [2] Y. Dubi and M. Di Ventra, Colloquium: Heat flow and thermoelectricity in atomic and molecular junctions, *Rev. Mod. Phys.* **83**, 131 (2011).
- [3] J. P. Pekola and B. Karimi, Colloquium: Quantum heat transport in condensed matter systems, *Rev. Mod. Phys.*

93, 041001 (2021).

- [4] G. E. W. Bauer, E. Saitoh, and B. J. v. Wees, Spin caloritronics, *Nat. Mater.* **11**, 391 (2012).
- [5] A. Fornieri and F. Giazotto, Towards phase-coherent caloritronics in superconducting circuits, *Nature Nanotech.* **12**, 944 (2017).
- [6] S.-Y. Hwang and B. Sothmann, Phase-coherent caloritronics with ordinary and topological josephson junctions, *The European Physical Journal Special Topics*

- 229**, 683 (2020).
- [7] B. Sothmann, R. Sánchez, and A. N. Jordan, Thermoelectric energy harvesting with quantum dots, *Nanotechnology* **26**, 032001 (2015).
- [8] G. Benenti, G. Casati, K. Saito, and R. S. Whitney, Fundamental aspects of steady-state conversion of heat to work at the nanoscale, *Physics Reports* **694**, 1 (2017).
- [9] L. d. C. Arrachea, Energy dynamics, heat production and heat–work conversion with qubits: towards the development of quantum machines, *Reports on Progress in Physics* (2023).
- [10] F. Giazotto and M. J. Martínez-Pérez, Phase-controlled superconducting heat-flux quantum modulator, *Applied Physics Letters* **101**, 102601 (2012).
- [11] F. Giazotto and M. J. Martínez-Pérez, The Josephson heat interferometer, *Nature* **492**, 401 (2012).
- [12] M. J. Martínez-Pérez and F. Giazotto, Fully balanced heat interferometer, *Applied Physics Letters* **102**, 092602 (2013).
- [13] A. Fornieri, C. Blanc, R. Bosisio, S. D’Ambrosio, and F. Giazotto, Nanoscale phase engineering of thermal transport with a Josephson heat modulator, *Nat Nano* **11**, 258 (2016).
- [14] A. Fornieri, G. Timossi, P. Virtanen, P. Solinas, and F. Giazotto, 0- π phase-controllable thermal Josephson junction, *Nature Nanotechnology* **12**, 425 (2017).
- [15] M. J. Martínez-Pérez and F. Giazotto, Efficient phase-tunable Josephson thermal rectifier, *Applied Physics Letters* **102**, 182602 (2013).
- [16] F. Giazotto and F. S. Bergeret, Thermal rectification of electrons in hybrid normal metal-superconductor nano-junctions, *Applied Physics Letters* **103**, 242602 (2013).
- [17] A. Fornieri, M. J. Martínez-Pérez, and F. Giazotto, A normal metal tunnel-junction heat diode, *Applied Physics Letters* **104**, 183108 (2014).
- [18] M. J. Martínez-Pérez, A. Fornieri, and F. Giazotto, Rectification of electronic heat current by a hybrid thermal diode, *Nat Nano* **10**, 303 (2015).
- [19] F. Giazotto, J. W. A. Robinson, J. S. Moodera, and F. S. Bergeret, Proposal for a phase-coherent thermoelectric transistor, *Appl. Phys. Lett.* **105**, 062602 (2014).
- [20] A. Fornieri, G. Timossi, R. Bosisio, P. Solinas, and F. Giazotto, Negative differential thermal conductance and heat amplification in superconducting hybrid devices, *Phys. Rev. B* **93**, 134508 (2016).
- [21] B. Sothmann, F. Giazotto, and E. M. Hankiewicz, High-efficiency thermal switch based on topological Josephson junctions, *New J. Phys.* **19**, 023056 (2017).
- [22] S.-Y. Hwang, F. Giazotto, and B. Sothmann, Phase-Coherent Heat Circulator Based on Multiterminal Josephson Junctions, *Phys. Rev. Applied* **10**, 044062 (2018).
- [23] M. Acciai, F. Hajiloo, F. Hassler, and J. Splettstoesser, Phase-coherent heat circulators with normal or superconducting contacts, *Phys. Rev. B* **103**, 085409 (2021), publisher: American Physical Society.
- [24] C. Guarcello, P. Solinas, A. Braggio, M. Di Ventra, and F. Giazotto, Josephson Thermal Memory, *Phys. Rev. Applied* **9**, 014021 (2018).
- [25] P. Solinas, R. Bosisio, and F. Giazotto, Microwave quantum refrigeration based on the Josephson effect, *Phys. Rev. B* **93**, 224521 (2016).
- [26] P. P. Hofer, M. Perarnau-Llobet, J. B. Brask, R. Silva, M. Huber, and N. Brunner, Autonomous quantum refrigerator in a circuit QED architecture based on a Josephson junction, *Phys. Rev. B* **94**, 235420 (2016).
- [27] F. Vischi, M. Carrega, E. Strambini, S. D’Ambrosio, F. S. Bergeret, Y. V. Nazarov, and F. Giazotto, Coherent transport properties of a three-terminal hybrid superconducting interferometer, *Phys. Rev. B* **95**, 054504 (2017).
- [28] H. L. Edwards, Q. Niu, and A. L. de Lozanne, A quantum-dot refrigerator, *Applied Physics Letters* **63**, 1815 (1993), <https://doi.org/10.1063/1.110672>.
- [29] H. L. Edwards, Q. Niu, G. A. Georgakis, and A. L. de Lozanne, Cryogenic cooling using tunneling structures with sharp energy features, *Phys. Rev. B* **52**, 5714 (1995).
- [30] J. R. Prance, C. G. Smith, J. P. Griffiths, S. J. Chorley, D. Anderson, G. A. C. Jones, I. Farrer, and D. A. Ritchie, Electronic Refrigeration of a Two-Dimensional Electron Gas, *Phys. Rev. Lett.* **102**, 146602 (2009).
- [31] S. Gasparinetti, F. Deon, G. Biasiol, L. Sorba, F. Beltram, and F. Giazotto, Probing the local temperature of a two-dimensional electron gas microdomain with a quantum dot: Measurement of electron-phonon interaction, *Phys. Rev. B* **83**, 201306 (2011).
- [32] A. V. Timofeev, M. Helle, M. Meschke, M. Möttönen, and J. P. Pekola, Electronic Refrigeration at the Quantum Limit, *Phys. Rev. Lett.* **102**, 200801 (2009).
- [33] L. Arrachea, M. Moskalets, and L. Martin-Moreno, Heat production and energy balance in nanoscale engines driven by time-dependent fields, *Phys. Rev. B* **75**, 245420 (2007).
- [34] M. Rey, M. Strass, S. Kohler, P. Hänggi, and F. Sols, Nonadiabatic electron heat pump, *Phys. Rev. B* **76**, 085337 (2007).
- [35] B. Cleuren, B. Rutten, and C. Van den Broeck, Cooling by Heating: Refrigeration Powered by Photons, *Phys. Rev. Lett.* **108**, 120603 (2012).
- [36] J. Brüggemann, S. Weiss, P. Nalbach, and M. Thorwart, Cooling a Magnetic Nanoisland by Spin-Polarized Currents, *Phys. Rev. Lett.* **113**, 076602 (2014).
- [37] J. P. Pekola, J. V. Koski, and D. V. Averin, Refrigerator based on the Coulomb barrier for single-electron tunneling, *Phys. Rev. B* **89**, 081309 (2014).
- [38] M. Nahum, T. M. Eiles, and J. M. Martinis, Electronic microrefrigerator based on a normal-insulator-superconductor tunnel junction, *Appl. Phys. Lett.* **65**, 3123 (1994).
- [39] M. M. Leivo, J. P. Pekola, and D. V. Averin, Efficient Peltier refrigeration by a pair of normal metal/insulator/superconductor junctions, *Appl. Phys. Lett.* **68**, 1996 (1996).
- [40] J. T. Muhonen, M. Meschke, and J. P. Pekola, Micrometre-scale refrigerators, *Rep. Prog. Phys.* **75**, 046501 (2012).
- [41] M. Rouco, T. T. Heikkilä, and F. S. Bergeret, Electron refrigeration in hybrid structures with spin-split superconductors, *Phys. Rev. B* **97**, 014529 (2018).
- [42] N. Linden, S. Popescu, and P. Skrzypczyk, How Small Can Thermal Machines Be? The Smallest Possible Refrigerator, *Phys. Rev. Lett.* **105**, 130401 (2010).
- [43] N. Brunner, N. Linden, S. Popescu, and P. Skrzypczyk, Virtual qubits, virtual temperatures, and the foundations of thermodynamics, *Phys. Rev. E* **85**, 051117 (2012).
- [44] A. Levy and R. Kosloff, Quantum absorption refrigerator, *Phys. Rev. Lett.* **108**, 070604 (2012).
- [45] N. Brunner, M. Huber, N. Linden, S. Popescu, R. Silva, and P. Skrzypczyk, Entanglement enhances cooling in

- microscopic quantum refrigerators, *Phys. Rev. E* **89**, 032115 (2014).
- [46] L. A. Correa, J. P. Palao, D. Alonso, and G. Adesso, Quantum-enhanced absorption refrigerators, *Sci. Rep.* **4**, 10.1038/srep03949 (2014).
- [47] L. A. Correa, Multistage quantum absorption heat pumps, *Phys. Rev. E* **89**, 042128 (2014).
- [48] D. Venturelli, R. Fazio, and V. Giovannetti, Minimal Self-Contained Quantum Refrigeration Machine Based on Four Quantum Dots, *Phys. Rev. Lett.* **110**, 256801 (2013).
- [49] O. Entin-Wohlman, Y. Imry, and A. Aharony, Enhanced performance of joint cooling and energy production, *Phys. Rev. B* **91**, 054302 (2015).
- [50] R. Sánchez, Correlation-induced refrigeration with superconducting single-electron transistors, *Appl. Phys. Lett.* **111**, 223103 (2017).
- [51] P. A. Erdman, B. Bhandari, R. Fazio, J. P. Pekola, and F. Taddei, Absorption refrigerators based on coulomb-coupled single-electron systems, *Physical Review B* **98**, 045433 (2018).
- [52] R. Wang, J. Lu, C. Wang, and J.-H. Jiang, Nonlinear effects for three-terminal heat engine and refrigerator, *Sci. Rep.* **8**, 2607 (2018).
- [53] R. Sánchez, P. Bursat, and A. L. Yeyati, Cooling by Cooper pair splitting, *Phys. Rev. B* **98**, 241414 (2018).
- [54] R. Hussein, M. Governale, S. Kohler, W. Belzig, F. Giazotto, and A. Braggio, Nonlocal thermoelectricity in a Cooper-pair splitter, *Phys. Rev. B* **99**, 075429 (2019).
- [55] D. Sánchez, R. Sánchez, R. López, and B. Sothmann, Nonlinear chiral refrigerators, *Phys. Rev. B* **99**, 245304 (2019).
- [56] A.-M. Daré, Comparative study of heat-driven and power-driven refrigerators with coulomb-coupled quantum dots, *Physical Review B* **100**, 195427 (2019).
- [57] S.-Y. Hwang, B. Sothmann, and D. Sánchez, Superconductor-quantum dot hybrid coolers, *Phys. Rev. B* **107**, 245412 (2023).
- [58] T.-S. Kim and S. Hershfield, Thermoelectric effects of an Aharonov-Bohm interferometer with an embedded quantum dot in the Kondo regime, *Phys. Rev. B* **67**, 165313 (2003).
- [59] O. Entin-Wohlman, Y. Imry, and A. Aharony, Three-terminal thermoelectric transport through a molecular junction, *Phys. Rev. B* **82**, 115314 (2010).
- [60] O. Entin-Wohlman and A. Aharony, Three-terminal thermoelectric transport under broken time-reversal symmetry, *Phys. Rev. B* **85**, 085401 (2012).
- [61] S.-Y. Hwang, J. S. Lim, R. López, M. Lee, and D. Sánchez, Proposal for a local heating driven spin current generator, *Applied Physics Letters* **103**, 172401 (2013).
- [62] P. Samuelsson, S. Kheradsoud, and B. Sothmann, Optimal Quantum Interference Thermoelectric Heat Engine with Edge States, *Phys. Rev. Lett.* **118**, 256801 (2017).
- [63] G. Haack and F. Giazotto, Efficient and tunable Aharonov-Bohm quantum heat engine, *Phys. Rev. B* **100**, 235442 (2019).
- [64] G. Blasi, F. Giazotto, and G. Haack, Hybrid normal-superconducting aharonov-bohm quantum thermal device, *Quantum Science and Technology* **8**, 015023 (2022).
- [65] A. Yacoby, M. Heiblum, D. Mahalu, and H. Shtrikman, Coherence and phase sensitive measurements in a quantum dot, *Phys. Rev. Lett.* **74**, 4047 (1995).
- [66] U. F. Keyser, C. Fühner, S. Borck, R. J. Haug, M. Bichler, G. Abstreiter, and W. Wegscheider, Kondo effect in a few-electron quantum ring, *Phys. Rev. Lett.* **90**, 196601 (2003).
- [67] H. Aikawa, K. Kobayashi, A. Sano, S. Katsumoto, and Y. Iye, Observation of “partial coherence” in an aharonov-bohm interferometer with a quantum dot, *Phys. Rev. Lett.* **92**, 176802 (2004).
- [68] M. Sigrist, T. Ihn, K. Ensslin, M. Reinwald, and W. Wegscheider, Coherent probing of excited quantum dot states in an interferometer, *Phys. Rev. Lett.* **98**, 036805 (2007).
- [69] R. Debbarma, H. Potts, C. J. Stenberg, A. Tsintzis, S. Lehmann, K. Dick, M. Leijnse, and C. Thelander, Effects of parity and symmetry on the aharonov-bohm phase of a quantum ring, *Nano Letters* **22**, 334 (2022).
- [70] Q.-f. Sun, J. Wang, and H. Guo, Quantum transport theory for nanostructures with rashba spin-orbital interaction, *Phys. Rev. B* **71**, 165310 (2005).
- [71] Q.-f. Sun and X. C. Xie, Bias-controllable intrinsic spin polarization in a quantum dot: Proposed scheme based on spin-orbit interaction, *Phys. Rev. B* **73**, 235301 (2006).
- [72] E. Vernek, N. Sandler, and S. E. Ulloa, Kondo screening suppression by spin-orbit interaction in quantum dots, *Phys. Rev. B* **80**, 041302 (2009).
- [73] J. S. Lim, M. Crisan, D. Sánchez, R. López, and I. Grosu, Kondo effect in spin-orbit mesoscopic interferometers, *Phys. Rev. B* **81**, 235309 (2010).
- [74] F. C. Wellstood, C. Urbina, and J. Clarke, Hot-electron effects in metals, *Phys. Rev. B* **49**, 5942 (1994).
- [75] H. Park, J. Park, A. K. L. Lim, E. H. Anderson, A. P. Alivisatos, and P. L. McEuen, Nanomechanical oscillations in a single-C60 transistor, *Nature* **407**, 57 (2000).
- [76] R. Leturcq, C. Stampfer, K. Inderbitzin, L. Durrer, C. Hierold, E. Mariani, M. G. Schultz, F. von Oppen, and K. Ensslin, Franck-Condon blockade in suspended carbon nanotube quantum dots, *Nat Phys* **5**, 327 (2009).
- [77] E. D. Minot, Y. Yaish, V. Sazonova, and P. L. McEuen, Determination of electron orbital magnetic moments in carbon nanotubes, *Nature* **428**, 536 (2004).
- [78] H. J. W. Haug and A.-P. Jauho, *Quantum Kinetics in Transport and Optics of Semiconductors*, Springer Series in Solid-State Sciences, Vol. 123 (Springer-Verlag, Berlin, 2008).
- [79] J. S. Lim, D. Sánchez, and R. López, Magnetoasymmetric transport in a mesoscopic interferometer: From the weak to the strong coupling regime, *Phys. Rev. B* **81**, 155323 (2010).
- [80] B. K. Agarwalla and D. Segal, Assessing the validity of the thermodynamic uncertainty relation in quantum systems, *Phys. Rev. B* **98**, 1554 (2018).
- [81] S. Kheradsoud, N. Dashti, M. Misiorny, P. P. Potts, J. Splettstoesser, and P. Samuelsson, Power, efficiency and fluctuations in a quantum point contact as steady-state thermoelectric heat engine, *Entropy* **21**, 10.3390/e21080777 (2019).